Electronic spectroscopy of intermediates involved in the conversion of methane to methanol by FeO^+

Fernando Aguirre, John Husband, Christopher J. Thompson, Kay L. Stringer, and Ricardo B. Metz[a)]
Department of Chemistry, University of Massachusetts, Amherst, Massachusetts 01003

(Received 30 October 2001; accepted 14 December 2001)

Specific ion–molecule reactions are used to prepare two intermediates of the $FeO^+ + CH_4$ reaction, and photodissociation of the jet-cooled intermediates is examined in the visible and near-ultraviolet using time-of-flight mass spectrometry. The photodissociation spectrum of the aquo iron carbene complex $[H_2C{=}Fe{-}OH_2]^+$ shows transitions to at least four excited electronic states in the $FeCH_2^+$ chromophore, with broad vibrational structure. Photoexcitation of the insertion intermediate $[HO{-}Fe{-}CH_3]^+$ leads to formation of $FeOH^+ + CH_3$ and also triggers the reaction to produce $Fe^+ + CH_3OH$. The photodissociation spectrum of $[HO{-}Fe{-}CH_3]^+$ presents a vibrationally resolved band involving progressions in the excited state Fe–C stretch, Fe–O stretch, and O–Fe–C bend. The change in the Fe–C bond length in $[HO{-}Fe{-}CH_3]^+$ and $[H_2C{=}Fe{-}OH_2]^+$ upon photoexcitation is calculated from a Franck–Condon analysis of the vibronic features observed. The analysis of the experimental results is aided by hybrid Hartree–Fock/density-functional (B3LYP) calculations on $[HO{-}Fe{-}CH_3]^+$ and $[H_2C{=}Fe{-}OH_2]^+$ performed to determine molecular parameters, and time-dependent density functional theory (TD-DFT) calculations on $FeCH_2^+$ to predict excited electronic states. © *2002 American Institute of Physics.*
[DOI: 10.1063/1.1448489]

I. INTRODUCTION

The direct oxidation of methane to an easily transportable liquid such as methanol has attracted great experimental and theoretical interest due to its importance as an industrial process and as the simplest model for alkane oxidation.[1,2] Although no direct, efficient methane–methanol conversion scheme has yet been developed,[1] significant advances have been made using iron-containing catalysts. Wang and Otsuka[3,4] have studied the direct oxidation of methane to methanol using $FePO_4$ as the catalyst and N_2O and H_2/O_2 as the oxidizing agents. However, despite the high catalytic selectivity obtained for methanol production, the reaction yield is low. In biological systems, the methane–methanol conversion is known to occur very efficiently. This oxidation is enzymatically catalyzed by methane mono-oxygenase (MMO), which contains nonheme iron centers enclosed in the active site.[5–7] In order to understand the chemistry of the MMO enzyme and model its reactivity to selectively oxidize methane at ambient temperature and pressure, close models of the enzyme's active site and several intermediates formed during the oxidizing catalytic cycle have been studied.[8–12] Recently, Lee and Lippard[11] described a synthetic model with a configuration, two Fe (III) atoms connected by two hydroxo- and one carboxylate bridging groups, that reproduces the configuration of the MMO core after the substrate has been oxidized.

In 1990 Schröder and Schwarz reported that gas-phase FeO^+ directly converts methane to methanol.[13] Reactions of gas-phase transition metal oxides with methane are thus a simple model system for the direct conversion of methane to methanol that is sufficiently small to be amenable to detailed experimental and theoretical study. As a result, these reactions have been extensively studied.[13–15] In the thermal gas-phase reaction of methane with FeO^+ there are two competitive pathways that lead to $FeOH^+ + CH_3$ (57%) and $Fe^+ + CH_3OH$ (41%). A minor pathway that leads to $FeCH_2^+ + H_2O$ (2%) has also been observed.[13] Three groups have collaborated in a critical study of this reaction over a range of pressures and collision energies.[15] They find that low collision energies and relatively high (0.5 mbar) buffer gas pressure favor the Fe^++methanol channel. To elucidate the mechanism for the production of methanol by FeO^+, Yoshizawa *et al.*[16–19] performed theoretical calculations using hybrid Hartree-Fock/density-functional (DFT) methods. They calculated that the reaction occurs via a $[HO{-}M{-}CH_3]^+$ insertion intermediate rather than a $[H{-}M{-}OCH_3]^+$ methoxy intermediate. In addition, Yoshizawa *et al.* suggest that the thermal reaction must undergo crossings between the sextet and quartet spin potential energy surfaces. To illustrate the conversion of methane to methanol by FeO^+, a schematic potential energy surface for the reaction is shown in Fig. 1. The reaction proceeds as follows: an encounter complex of the reactants $[H_4C\cdots FeO]^+$ (**1**) is initially produced by an electrostatic interaction between FeO^+ and methane. Then, an insertion intermediate $[HO{-}Fe{-}CH_3]^+$ (**2**) is produced by σ-metathesis between a C–H bond of methane and the Fe–O bond. The migration of a methyl group in **2** produces the iron/methanol exit channel complex $[Fe(CH_3OH)]^+$ (**3**),

a)Author to whom correspondence should be addressed. Electronic mail: rbmetz@chemistry.umass.edu

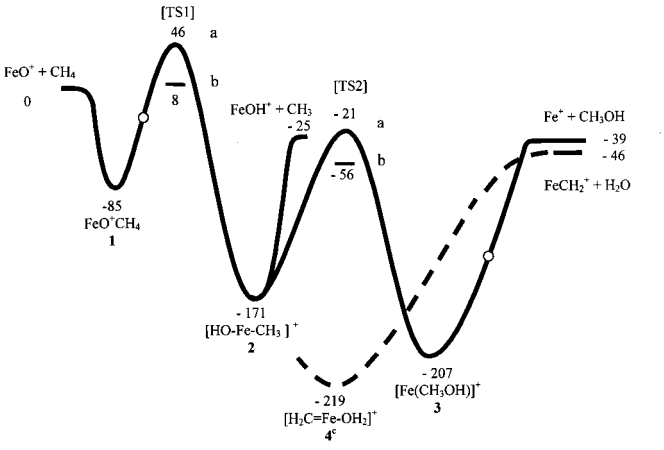

FIG. 1. Schematic potential energy surface for the conversion of methane to methanol by FeO^+. All minima were calculated using the Becke–Lee–Yang–Parr HF/DFT method (B3LYP). To outline the entire potential energy surface, energies (kJ mol^{-1}) of the transition states (TS) calculated by Yoshizawa *et al.* (Ref. 19) in the sextet (a) and quartet spin states (b), relative to the preceding reaction intermediate, are also included. The steps where crossings between high-spin and low-spin potentials occur are marked with circles. The B3LYP energies for the minor pathway (c) $[H_2C{=}Fe{-}OH_2]^+(^4A')\rightarrow FeCH_2^+(^4B_1)+H_2O(^1A_1)$ are also included for a complete description of the reaction of methane with FeO^+. The relative energy between the products of the methanol and water reaction pathways is derived from thermodynamic values.

which subsequently dissociates to produce $Fe^+ + CH_3OH$. Yoshizawa *et al.* also suggest that the competitive pathway that leads to $FeOH^+ + CH_3$ is derived from the cleavage of the Fe–C bond in **2**. Calculations performed by Schröder *et al.*[20] at the MP2/ECP-DZ level of theory suggest that the minor channel, $FeO^+ + CH_4 \rightarrow FeCH_2^+ + H_2O$, is derived from the dissociation of an aquo iron carbene intermediate $[H_2C{=}Fe{-}OH_2]^+$ (**4**), which is produced from **2**. The energies of this minor channel calculated at the B3LYP level are also included in Fig. 1, relative to the experimental energy difference between the products of the methanol and water reaction pathways calculated from standard thermodynamic values.[21,22] Thus, on the basis of these theoretical results, $[HO{-}Fe{-}CH_3]^+$ has been suggested to be the most important intermediate in methane–methanol conversion by FeO^+. Experiments have also suggested the key role of the insertion intermediate. In an elegant series of collisional activation mass spectrometry experiments, Schröder *et al.*[20] present clear evidence for the existence of the reactant and product complexes **1** and **3** as well as the insertion and aquo iron carbene intermediates **2** and **4**. In addition, Armentrout and co-workers[23] suggest that an analogous insertion intermediate, $[HO{-}Co{-}CH_3]^+$, plays a key role in the gas-phase conversion of methane to methanol by CoO^+. Therefore, on the basis of these experimental and theoretical results, the intrinsic characterization of the reaction intermediates, in particular $[HO{-}M{-}CH_3]^+$, is quite interesting.

Over the last decade, our understanding of the ground electronic state of transition-metal-containing systems has been greatly enhanced by DFT (B3LYP) calculations.[19,24–26] The application of this methodology to the prediction of excited electronic states, by using the time-dependent (TD-DFT) scheme, has mostly concerned closed-shell organic[27,28] or inorganic[29,30] molecules and few calculations have been performed on open-shell systems containing transition metals.[31] Using TD-DFT, Borowsky and Broclawik[31] predicted excited states of VO ($^4\Sigma^-$) and MoO ($^5\Pi$) that are in excellent agreement with both experimental results and calculations performed at higher levels of theory. The ease and low computational cost of TD-DFT calculations make it an attractive tool for the study of excited electronic states, if further studies confirm its reliability. So, additional TD-DFT calculations on other open-shell transition metal containing systems are highly desirable to validate this methodology.

As part of an on-going effort to characterize the species involved in the gas-phase methane–methanol conversion by first-row transition-metal oxide cations, we studied the reaction intermediates $[H_2C{=}Fe{-}OH_2]^+$ and $[HO{-}Fe{-}CH_3]^+$ by photodissociation. On the basis of our experimental results and calculations performed at the B3LYP and TD-B3LYP level, excited state vibrational frequencies as well as geometry changes upon photoexcitation in $[H_2C{=}Fe{-}OH_2]^+$ and $[HO{-}Fe{-}CH_3]^+$ will be discussed.

II. EXPERIMENT AND THEORY

A. General procedure

The photofragment spectrometer used in this study has been described in detail previously.[32] Iron cations are generated by laser ablation of a rotating and translating rod (Fe, Sigma-Aldrich, 99.98% pure). Ablated Fe^+ reacts with a suitable organic precursor seeded in the carrier gas (He, UHP grade, 99.999%) to produce the ion of interest. The precursors used and methods applied to characterize the intermediates are described in Sec. III. Ions produced in the source expand supersonically into vacuum, then are skimmed, accelerated to 1800 V kinetic energy, and re-referenced[33] to ground potential prior to entering the field-free flight tube. Photoexcitation of the mass-selected cation of interest is accomplished at the turning point of the reflectron using the fundamental and/or frequency-doubled output of a tunable Nd:YAG-pumped dye laser. The laser line width is <0.1 cm^{-1} for the dye fundamental and <0.2 cm^{-1} for the frequency-doubled output. The masses of charged dissociation fragments are determined by their subsequent flight times to a 40 mm diameter dual microchannel plate detector, thus identifying dissociation channels. The photodissociation spectrum of a specific channel is obtained by monitoring the yield of the corresponding fragment ion as a function of wavelength and normalizing to parent ion signal and laser power. Photodissociation of the intermediates studied is linear with laser fluences up to 100 mJ cm^{-2}; typically a fluence of 50 mJ cm^{-2} was used. The two-photon dissociation of $FeCH_2^+$ was produced by focusing the fundamental of the tunable Nd:YAG-pumped dye laser using a 50-cm focal length lens, giving laser fluence of ~ 1 J cm^{-2}. The laser wavelength is calibrated using the known photoacoustic spectrum of water.[34]

B. Calculations

All calculations were carried out using the Becke–Lee–Yang–Parr HF/DFT method (B3LYP), using the GAUSSIAN 98

ab initio program package.[35] Optimized geometries were calculated using the diffuse 6-311+G(d,p) basis set on all the atoms, except for calculations on $[H_2C{=}Fe{-}OH_2]^+$, where no diffuse functions were included. Vibrational frequencies were systematically computed in order to ensure that all optimized geometries correspond to a local minimum. Single-point energies were calculated at each optimized geometry using the 6-311+G($3df,2dp$) basis set on hydrogen, oxygen, and carbon, and the 6-311+G(d,p) basis set on iron. Computed $\langle S^2 \rangle$ values confirmed that spin contamination is minimal, except for $[FeCH_2]^+$ and $[H_2C{=}Fe{-}OH_2]^+$, where small contamination was found. Details of this contamination, as well as calculations to estimate the potential barrier to linearity of $[HO{-}Fe{-}CH_3]^+$, will be presented in Sec. III.

Time-dependent density functional theory (TD-DFT) calculations on $[FeCH_2]^+$ were performed at the B3LYP level using the 6-311+G(d,p) basis set on all the atoms. The excited state potential energy curves were constructed by scanning the Fe–C bond length and starting TD calculations from the converged ground state density at each bond length. The calculated curves were subsequently fitted to a Morse potential profile from which molecular parameters for the excited state were derived.

III. RESULTS AND DISCUSSION

A. Precursors

The potential energy surface for the $FeO^+ + CH_4$ reaction, shown in Fig. 1, has several local minima that correspond to intermediates that, once formed and supersonically cooled, are stable on the time scale of our experiment. However, because these intermediates are all isomers, they cannot be separated using simple mass spectrometry and so they must be generated in a clean fashion in the gas phase. Schröder *et al.*[20] produced several intermediates of the $FeO^+ + CH_4$ reaction by reacting Fe^+ with a variety of neutral molecules in an ion cyclotron resonance spectrometer (ICR). The intermediates were identified based on fragment ions produced following collision-induced dissociation (CID). We tried to synthesize the intermediates of interest using the same precursors as Schröder *et al.*[20] and characterized the intermediates formed by their photodissociation products and photodissociation spectrum. Although conditions in our ion source are very different from those used by Schröder *et al.*, we generally observe the same reaction products.

In a first attempt to generate $[HO{-}Fe{-}CH_3]^+$ (**2** in Fig. 1), methanesulfonic acid (CH_3SO_3H, Fluka AG, >98% pure) was used but no ion signal at $m/z=88$ was obtained due to the low vapor pressure of this precursor. Subsequently, we used n-propanol (C_3H_7OH, Mallinckrodt, 99.9% pure) which is reported[20] to produce a mixture of **2** and $[H_2C{=}Fe{-}OH_2]^+$ (**4** in Fig. 1), in a 10:1 ratio. The reaction of this precursor with Fe^+ mostly produces $[FeC_3H_6]^+$, but a moderate signal at $m/z=88$ is also obtained. Photodissociation of this mixture in the near-ultraviolet produces three distinguishable peaks corresponding to the loss of methyl radical, water, and methanol. Of these channels, loss of water is the only channel that remains active into the visible. Loss of H_2O is characteristic of $[H_2C{=}Fe{-}OH_2]$, while loss of CH_3 and CH_3OH is characteristic of $[HO{-}Fe{-}CH_3]^+$. The photodissociation spectrum for each channel is obtained by monitoring the yield of a mass-selected photofragment as a function of the dissociation laser wavelength. Thus, the individual characterization of these isomeric intermediates is made possible by the presence of distinct dissociation channels. To confirm that the distinct dissociation channels are derived from **2** and **4**, acetic acid (CH_3COOH, Fisher Scientific, 99.9% pure) was used as a precursor. Schröder *et al.* report the production of **2** and **4** in a 1:4 ratio using this reaction.[20] In contrast to the reaction with n-propanol, the reaction of Fe^+ with acetic acid efficiently produces ions with $m/z=88$. Photodissociation of these ions gives a higher yield of $FeCH_2^+ + H_2O$, which indicates that **4** is the major isomer produced.

In an attempt to generate the exit channel complex $[Fe(CH_3OH)]^+$, methanol was used as a precursor. The reaction of Fe^+ with methanol efficiently produces ions with the desired m/z ratio, which in the near-ultraviolet dissociate by loss of methyl radical, as the major channel, and loss of methanol. Although an analogous fragmentation pattern is observed in the collisional activation study of $[HO{-}Fe{-}CH_3]^+$ reported by Schröder *et al.*,[20] they observed the loss of methanol as the major channel. The dissociation spectra of ions produced by the reaction of Fe^+ with methanol, monitoring either channel, are identical to those obtained from the dissociation of $[HO{-}Fe{-}CH_3]^+$ produced either with n-propanol or acetic acid. On the basis of these results, under our experimental conditions the reaction of Fe^+ with methanol leads to formation of $[HO{-}Fe{-}CH_3]^+$ as a major product. A detailed analysis of this reaction will be presented in the discussion of $[HO{-}Fe{-}CH_3]^+$.

B. Aquo iron carbene intermediate $[H_2C{=}Fe{-}OH_2]^+$

In the reaction of FeO^+ with CH_4, $[H_2C{=}Fe{-}OH_2]^+$ is the exit channel complex that leads to the formation of $FeCH_2^+ + H_2O$. In this complex, the $Fe^+{-}OH_2$ interaction is expected to be basically electrostatic, which suggests that the $FeCH_2^+$ moiety is the chromophore in the electronic spectroscopy of $[H_2C{=}Fe{-}OH_2]^+$. As described above, $[H_2C{=}Fe{-}OH_2]^+$ was efficiently generated by the reaction of Fe^+ with acetic acid. Figure 2 shows the photodissociation spectrum of the unique channel $[H_2C{=}Fe{-}OH_2]^+ + h\nu \rightarrow FeCH_2^+ + H_2O$ from 13 700 to 30 000 cm^{-1}, and the upper trace in Fig. 3 highlights the low-energy portion of the spectrum. The dissociation channel $[H_2C{=}Fe{-}OH_2]^+ + h\nu \rightarrow Fe(H_2O) + CH_2^+$ is not observed even at energies above $D_o^0(Fe^+{-}CH_2)$.[36] Figure 2 shows transitions to at least four excited electronic states, some exhibiting vibrational structure. Among these transitions, the most distinguishable is the series of four ~300-cm^{-1} wide peaks separated by 470 cm^{-1}, observed at the red end of the spectrum. The remaining features are the two peaks near 16 000 cm^{-1}, separated by 510 cm^{-1}, and the two intense, poorly resolved bands centered at 17 400 and 19 500 cm^{-1}, respectively. No resolved features are observed to higher energy except a sharp

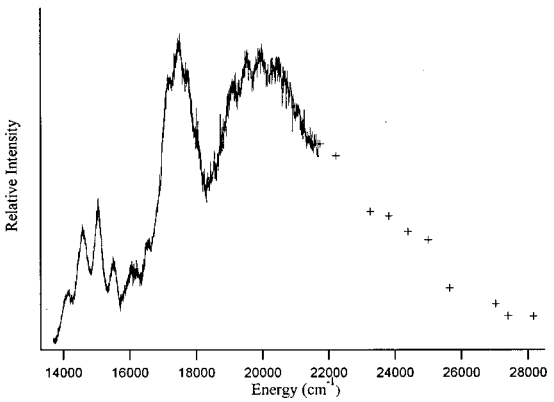

FIG. 2. Photodissociation spectrum of $[H_2C{=}Fe{-}OH_2]^+ + h\nu \rightarrow FeCH_2^+ + H_2O$. Above 21 500 cm^{-1}, the spectrum was obtained at ~600 cm^{-1} intervals and is indicated with (+) symbols.

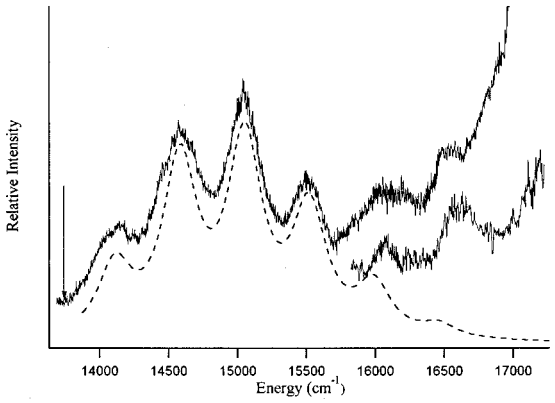

FIG. 3. Expanded portion of the photodissociation spectrum of $[H_2C{=}Fe{-}OH_2]^+$ (upper trace). The vertical arrow at 13 700±200 cm^{-1} indicates the spectroscopic onset for photodissociation. The simulated spectrum generated using a harmonic approximation of the Fe–(CH_2) stretching mode is shown with a dashed line. The lower solid trace from ~16 000 to 17 500 cm^{-1} shows the resonant two-photon dissociation spectrum of $FeCH_2^+$, obtained by monitoring Fe^+. The energy shown for the two-photon spectrum is the energy of one photon, shifted 1740 cm^{-1} to higher energy. This shift is to facilitate comparison with the spectrum of $[H_2C{=}Fe{-}OH_2]^+$ and is due to the difference in solvation energies of the ground and excited state of $FeCH_2^+$ by H_2O.

increase in the dissociation yield above 33 000 cm^{-1}. Analysis of the series of four peaks separated by 470±20 cm^{-1} gives a normal mode displacement of 0.53±0.05 Å $amu^{1/2}$, which corresponds to an Fe–C bond length change of 0.16 ±0.02 Å. This displacement of the Fe–C bond is obtained using the calculated Fe–(CH_2) mode for the ground state of $[H_2C{=}Fe{-}OH_2]^+$, in which it is a nearly pure Fe–C stretch. Details of calculations on $[H_2C{=}Fe{-}OH_2]^+$ are given below. The simulated spectrum (dashed line in Fig. 3) is generated by convoluting Franck–Condon factors[37] calculated for harmonic potentials for the ground- and excited state with a Lorentzian function with a width of 300 cm^{-1}. The observed dissociation threshold at 13 700±200 cm^{-1} implies an *upper limit* $D_o^0(H_2CFe^+{-}OH_2) \leqslant 164 \pm 2$ kJ mol^{-1}.

In view of the several low-lying excited states of $FeCH_2^+$ revealed by the photodissociation of $[H_2C{=}Fe{-}OH_2]^+$, we studied $FeCH_2^+$ using resonant two-photon dissociation. One photon promotes the parent ions to a particular vibrational–rotational state in a low-lying electronic state and the second photon excites the molecule to a higher electronic state from which it dissociates. Features obtained in the resonant two-photon dissociation spectrum are characteristic of the low-lying electronic state. The two-photon dissociation spectrum of $FeCH_2^+$ (the less intense trace of Fig. 3), presents two peaks separated by 510 cm^{-1} followed by a steady increase in the dissociation yield to higher energy. The two-photon spectrum has been shifted 1740 cm^{-1} to higher energy to facilitate comparison with the one-photon dissociation spectrum of $[H_2C{=}Fe{-}OH_2]^+$. The low-energy vibrational features observed in the spectrum of $[H_2C{=}Fe{-}OH_2]^+$ are not observed in the two-photon spectrum because they occur at energies below the two-photon dissociation threshold of $FeCH_2^+$. The similarity between the peaks in the two-photon spectrum of $FeCH_2^+$ and those in the spectrum of $[H_2C{=}Fe{-}OH_2]^+$ near 16 000 cm^{-1} indicates that the observed electronic/vibrational features in the spectrum of $[H_2C{=}Fe{-}OH_2]^+$ correspond to transitions in the $FeCH_2^+$ chromophore. The shift to the blue of the two-photon spectrum indicates that H_2O solvates $FeCH_2^+$ more strongly in the ground state than in the excited state. Since the appearance of the peaks in both spectra is very similar, the broadening observed in the spectrum of $[H_2C{=}Fe{-}OH_2]^+$ is presumably due to internal conversion in the excited state of $FeCH_2^+$ rather than to the photodissociation lifetime of $[H_2C{=}Fe{-}OH_2]^+$.

To obtain an estimated $D_o^0(H_2CFe^+{-}OH_2)$ value, calculations were performed at the B3LYP level of theory. Our recent calculations[26] on the dissociation of $[HONi{-}OH_2]^+$, in addition to the calculations on cationic methylene complexes MCH_2^+ performed by Koch and co-workers,[38] show that density functional theory is well suited to the calculation of dissociation energies for ions of this nature. Because $[H_2C{=}Fe{-}OH_2]^+$ is best described as $FeCH_2^+$ ligated by water, it is likely that under our experimental conditions this ion, like $FeCH_2^+$, is produced in the quartet spin state. The $^4A'$ ground state of $[H_2C{=}Fe{-}OH_2]^+$ is calculated to have a slightly distorted C_{2v} symmetry with Fe–O and Fe–C bond lengths of 2.03 and 1.86 Å, respectively, with the carbon, iron, and oxygen atoms lying almost in the same plane. Comparison with the optimized geometry of $FeCH_2^+$, also calculated at the B3LYP level, shows that the $FeCH_2^+$ in $[H_2C{=}Fe{-}OH_2]^+$ is not significantly altered by the addition of the water molecule. The Fe–C bond length is elongated only by ~0.01 Å, while the C–H bond lengths remain unchanged. Calculations of $[H_2C{=}Fe{-}OH_2]^+$ constrained to C_{2v} symmetry give a significant elongation in the Fe–C bond length (~7%). This change is unusual considering the $[H_2C{=}Fe{-}OH_2]^+$ is produced by the electrostatic interaction between $FeCH_2^+$ and water. In contrast to similar calculations of other iron complexes, calculations performed on both $FeCH_2^+$ and $[H_2C{=}Fe{-}OH_2]^+$ show a spin contamination of ~13% ($\langle S^2 \rangle = 4.2$). However, from this calculation a $D_o^0(H_2CFe^+{-}OH_2)$ value of 167 kJ mol^{-1} is obtained, which is in excellent agreement with our experimental upper bound of 164±2 kJ mol^{-1}. To test the reliability of this method, the dissociation $FeCH_2^+(^4B_1) \rightarrow Fe^+(^6D) + CH_2(^3B_1)$ was also

calculated at the same level of theory. The calculated value $D_o(Fe^+-CH_2)=352$ kJ mol^{-1} is in good agreement with the experimental values of 341 ± 4 kJ mol^{-1} and $\leqslant 342\pm2$ kJ mol^{-1} reported by Armentrout and co-workers[22] and Husband *et al.*,[36] respectively, and with the B3LYP value of 348 kJ mol^{-1} calculated by Koch and co-workers.[38] Thus, on the basis of these results, the spin contamination observed in the calculations of $[H_2C{=}Fe{-}OH_2]^+$ and $[FeCH_2]^+$ does not seem to adversely affect the results.

To identify the transitions observed in the spectrum of $[H_2C{=}Fe{-}OH_2]^+$, the understanding of the electronic structure of the chromophore $FeCH_2^+$ becomes essential. During the past two decades $FeCH_2^+$ has been the subject of numerous experimental and theoretical studies.[36,39–41] However, only its ground state has been extensively studied and few attempts have been made to characterize excited states. Musaev and Morokuma,[40] at the MR-SDCI-CASSCF(9/10) +Davidson correction level of theory, predicted that the ground state of $FeCH_2^+$ is a nearly degenerate pair ($^4B_2$ and $^4B_1$). In addition, a low-lying $^4A_2$ state is calculated ~8 kJ mol^{-1} above the ground state while two doublet states ($^2A_1$ and $^2A_2$) are about 105–147 kJ mol^{-1} higher in energy. To the best of our knowledge, quartet excited states, other than the low-lying $^4A_2$, have not been calculated for $FeCH_2^+$. Therefore, we performed calculations on $FeCH_2^+$ using time-dependent density functional theory (TD-DFT). To date, few TD-DFT calculations have been carried out on open-shell transition-metal-containing systems, so the reliability of this method in the prediction of excited states is still uncertain. Recent TD-DFT calculations on VO and MoO performed by Broclawik and Borowski[31] predict adiabatic excitation energies with a mean absolute error of ~1500 cm^{-1} relative to experimental values. Similar calculations performed by our group on CrF, MnO, and FeO^+ give similar deviations for the excitation energies.[42] TD-DFT calculations performed on $FeCH_2^+(^4B_1)$ predict two electronic transitions which are in close agreement with the electronic features observed in the spectrum of $[H_2C{=}Fe{-}OH_2]^+$. A transition to a low-lying $^4A_1$ excited state is calculated at 13 500 cm^{-1} with an oscillator strength $f=10^{-3}$. A second transition, with an f value one order of magnitude higher, is calculated at 20 800 cm^{-1} and reaches a $^4B_1$ excited state. The calculated excitation energy of 13 500 cm^{-1} is in excellent agreement with the vibrationally resolved transition observed above 13 700 cm^{-1}, while the other transitions can account for the intense band centered at 19 500 cm^{-1}. To derive molecular parameters of these excited states, their potential energy curves were constructed by scanning the Fe–C bond length and performing TD calculations from the converged ground state density at each bond length. By fitting the calculated potential energy curves to a Morse profile, the equilibrium bond length and vibrational frequency of the $^4A_1$ and $^4B_1$ excited state were derived. For the $^4A_1$ excited state an Fe–C stretch frequency of 511 ± 40 cm^{-1} is obtained, while the Fe–C bond length is predicted to increase by 0.20 ± 0.02 Å. These results are in good agreement with the Fe–C bond length change of 0.16 ± 0.02 Å and vibrational frequency of 470 ± 20 cm^{-1} derived from the Franck–Condon analysis of the vibrationally resolved progression shown in Fig. 3.

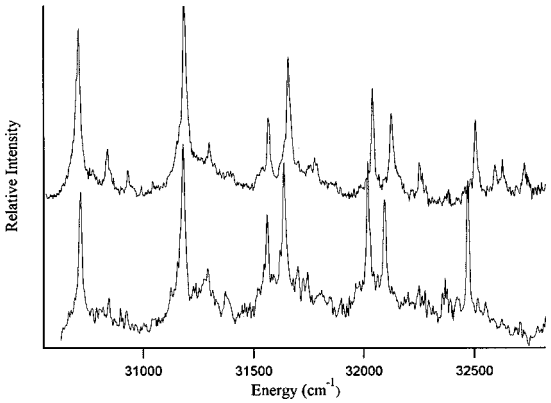

FIG. 4. Photodissociation spectrum of $[H_3C{-}Fe{-}OH]^+$ (upper trace) and $[D_3C{-}Fe{-}OH]^+$ (lower trace) recorded by monitoring $FeOH^+$. A similar spectrum is obtained by monitoring Fe^+.

This result shows that the spectroscopic study of $[H_2C{=}Fe{-}OH_2]^+$ is a feasible way to probe the spectroscopy of $FeCH_2^+$ at energies below $D_o^0(Fe{-}CH_2)^+$ (spectator spectroscopy).[43,44] The elongation in the Fe–C bond length is due to promoting an electron from the $2b_1$ Fe^+-CH_2 π-bonding orbital to the slightly antibonding $Fe-CH_2$ $7a_1$ orbital. Since the ground state of $FeCH_2^+$ has been calculated as a nearly degenerate pair ($^4B_1$ and $^4B_2$) with a low-lying $^4A_1$ excited state,[40] transitions from $^4B_2$ or $^4A_1$ to the calculated TD excited states may account for the remaining electronic features observed in the spectrum of $[H_2C{=}Fe{-}OH_2]^+$.

C. Insertion intermediate $[HO{-}Fe{-}CH_3]^+$

One interesting aspect of the photodissociation of $[HO{-}Fe{-}CH_3]^+$ is the competition between the reaction to produce $Fe^+ + CH_3OH$ and the nonreactive channel $FeOH^+ + CH_3$. By monitoring either Fe^+ or $FeOH^+$ as a function of the dissociation laser wavelength, the photodissociation spectrum shown in Fig. 4 is obtained. At higher dissociation energies, the dissociation yields for both channels increase and some broad, unresolved features are observed. The $Fe^+/FeOH^+$ ratio is ~0.8 at each large peak and decreases to ~0.5 away from a resonance peak. Farrar and co-workers[45] observe a similar effect in the photodissociation of $[Sr(CH_3OH)]^+$, where the yield of the reactive channel (formation of $SrOH^+ + CH_3$) is enhanced at each resonance, at the expense of the nonreactive ($Sr^+ + CH_3OH$) channel. This behavior is likely due to the presence of long-lived resonance states (which lead to dissociation) superimposed on a broad absorption due to short-lived, nonreactive states.

Prior to the detailed analysis of the photodissociation spectrum of $[HO{-}Fe{-}CH_3]^+$, a review of the gas-phase reaction used to generate this intermediate has to be done. As mentioned before, $[HO{-}Fe{-}CH_3]^+$ was generated by reacting Fe^+ with acetic acid, n-propanol, or methanol. The same photodissociation spectrum, as shown in Fig. 4, was obtained for both the methyl radical and methanol channel for $m/z=88$ ions generated with any of these precursors. Schröder *et al.*[20] report the formation of $[HO{-}Fe{-}CH_3]^+$ using acetic acid and n-propanol, but reported that reaction with methanol

TABLE I. Observed transitions of $[HO–Fe–CH_3]^+$ and $[HO–Fe–CD_3]^+$. All transitions are produced from the vibrationless ground state. Positions of vibronic peaks are given relative to the respective origin.

Relative energy [cm^{-1}]			
$[HO–Fe–CH_3]^+$	$[HO–Fe–CD_3]^+$	Assignment	Isotopic ratio $\rho=D/H$
30 706.8	30 717.3	Origin	$\Delta E=10.5$ cm^{-1}
132.1	126.5	14^1	
475.4	460.7	11^1	0.969
591.1	573.9	$11^1 14^1$	
860.9	844.5	8^1	0.981
949.3	919.4	11^2	0.969
1 047.3	1 008.2	$11^2 14^1$	
1 332.6	1 300.6	$11^1 8^1$	
1 417.5	1 374.6	11^3	0.970
1 687.6	1 659.7	8^2	0.984
1 798.8	1 752.9	$11^2 8^1$	
2 259.8	2 197.5	$11^3 8^1$	

produces $[Fe(CH_3OH)]^+$. Allison and Ridge,[46] using double-resonance ion cyclotron resonance spectroscopy, find that the reaction of Fe^+ with methanol produces $[HO–Fe–CH_3]^+$. Under our experimental conditions, the reaction of Fe^+ with methanol leads to the formation of $[HO–Fe–CH_3]^+$ as a major product. The photodissociation spectrum of $[HO–Fe–CH_3]^+$ shows well-resolved vibrational structure, so it is useful to also study $[HO–Fe–CD_3]^+$, which is produced by reacting Fe^+ with CD_3OH. As will be discussed in more detail below, isotopic shifts in the photodissociation spectrum are consistent with a $[HO–Fe–CH_3]^+$ structure. Thus, on the basis of these results, it is likely that either the transition state TS2 in the sextet spin state shown in Fig. 1 lies below $Fe^+ + CH_3OH$, or the reaction undergoes spin crossing to produce $[HO–Fe–CH_3]^+$ in the quartet spin state. The calculated isotopic shifts in the sextet spin state are consistent with the observed shifts in the photodissociation spectrum of $[HO–Fe–CH_3]^+$ (see the supporting information).[47] Therefore, for the analysis of the spectrum we assume that $[HO–Fe–CH_3]^+$ is produced in the sextet spin state.

The spectra shown in Fig. 4 were obtained by optimizing source conditions to minimize vibrational hot and sequence bands, leading to narrow, well-resolved peaks in the photodissociation spectrum. The vibrational peaks are ~ 20 cm^{-1} wide, which gives a lower limit to the excited state lifetime of ~ 0.27 ps. However, several peaks are slightly asymmetric, tailing to low energy. This is likely due to unresolved rotational structure, implying that the true upper state lifetime is somewhat longer than 0.27 ps. All observed features can be assigned as originating in the vibrationless ground state. The lowest energy peak observed at $30\,707 \pm 5$ cm^{-1} is assigned to the vibronic origin, as high-resolution scans down to 29 800 cm^{-1} show no additional peaks. The remaining structure is due to progressions in three vibrations in the excited state. The first progression consists of five vibronic peaks, the most intense in the spectrum, separated by approximately 475 cm^{-1}. Residing at 858 cm^{-1} above the origin a second progression is observed, almost half as intense as the first progression. A third, less intense, progression is observed 123 cm^{-1} from the band origin. To identify the vibrational modes associated with each progression, we studied the deuterated intermediate $[HO–Fe–CD_3]^+$. The deuterated complex dissociates without any isotopic scrambling by forming Fe^+ and $FeOH^+$. As seen in Fig. 4, the observed peaks are sufficiently narrow that the isotopic shift in the photodissociation spectrum of the isotopomers is observed. The positions of observed peaks are listed in Table I, along with the isotopic frequency ratio $\rho = \nu_{[HO–Fe–CD_3]^+} / \nu_{[HO–Fe–CH_3]^+}$.

TABLE II. Experimental and calculated vibrational frequencies of $[HO–Fe–CH_3]^+$ and isotopic shift of $[HO–Fe–CD_3]^+$.

	Experimental excited state		Calculated ground state	
Vibrational mode	Frequency (cm^{-1})	Isotopic shift ρ[b]	Frequency[a] (cm^{-1})	Isotopic shift[b] ρ
Fe–C stretch ν_{11}	478±3	0.969	480	0.965
Fe–O stretch ν_8	860.9±3	0.981	772	0.997
O–Fe–C bend ν_{14}	132.1±3		109	0.954
Barrier to linearity			1523[c]	

[a]Values calculated at the B3LYP/6-311+G(d,p) level.
[b]Frequency ratio $\rho = \nu_{[HO–Fe–CD_3]^+} / \nu_{[HO–Fe–CH_3]^+}$.
[c]Calculated at the B3LYP/6-311G(d,p) level by scanning the O–Fe–C angle in $[HO–Fe–CH_3]^+$.

In assigning the experimentally observed vibrational features, it is extremely useful to know the vibrational frequencies of $[HO–Fe–CH_3]^+$. Because the ground- and excited state vibrational frequencies of the insertion intermediate are not known, ground state frequencies were calculated at the B3LYP level of theory. Although calculations are for the ground electronic state, the molecular parameters obtained are useful in the assignment of the frequencies in the excited state. Table II shows the calculated frequencies and isotopic shifts of the three vibrational modes active in the photodissociation spectrum of $[HO–Fe–CH_3]^+$. All of the calculated vibrational frequencies of $[HO–Fe–CH_3]^+$ and $[HO–Fe–CD_3]^+$ are listed in the supporting information.[47]

The main progression observed has a frequency (ω_e') of 481 ± 1.0 cm^{-1} and anharmonicity ($\omega_e x_e'$) of 2.6 ± 0.2 cm^{-1}, and is assigned to the Fe–C stretch (ν_{11}). To simulate this progression, Franck–Condon factors (FCF) were calculated using a harmonic potential for the ground state, with the calculated frequency, while a Morse potential was used for the excited state. The same reduced mass was used for both states. The Franck–Condon analysis indicates a normal mode displacement of 0.44 ± 0.03 Å $amu^{1/2}$, which corresponds to an Fe–C bond length change of 0.13 ± 0.01 Å, using as the calculated normal mode for ν_{11} the ground state of $[HO–Fe–CH_3]^+$, in which it is a nearly pure Fe–C stretch. With reduced intensity, a progression at 861 cm^{-1} is also observed, which is assigned to the Fe–OH stretch (ν_8). The rapid change in the peak intensities suggests a small change in the Fe–OH bond length in the excited state. A normal mode displacement of 0.20 ± 0.02 Å $amu^{1/2}$ is obtained from the Franck–Condon analysis, which leads to an Fe–O bond length change of 0.05 ± 0.01 Å. The small peaks with spacing of $\sim$130 cm^{-1} are assigned to a progression in the O–Fe–C bend (ν_{14}). To simulate this progression, ν_{14} was treated as an independent harmonic vibration and the same reduced mass was used for the ground- and excited states. The best-fit harmonic potential for the excited state gives a displacement of 0.35 ± 0.10 Å $amu^{1/2}$ along the bend normal coordinate, which corresponds to a change of 4.4 ± 1.3 deg in the O–Fe–C angle. Intensities and positions calculated using harmonic potentials were used to simulate the spectrum shown in Fig. 5. The spectrum shows that there is a coupling between the bend and the Fe–C stretch in the excited state, because the bend frequency and intensity depends on the number of quanta in the Fe–C stretch. To explore the bend potential, a relaxed potential energy surface scan along the O–Fe–C angle was calculated at the B3LYP/6-311G(d,p) level. At each step of the scan, the O–Fe–C angle was fixed while the remaining molecular parameters were optimized. The resulting potential has a barrier to linearity of 1500 cm^{-1} and shows a coupling between the Fe–C stretch and the bend (see the supporting information).[47] The optimized Fe–O bond length is nearly independent of the bend angle, while the Fe–C bond length is significantly reduced as the molecule becomes more linear. Thus, the simulation of the progression in ν_{14} could be improved by including coupling between ν_{11} and ν_{14} in the excited state. However, considering the few peaks observed in the bend progression and their low intensity, we have simulated the remaining peaks in the spectrum of $[OH–Fe–CH_3]^+$, which are due to combinations of ν_8, ν_{11}, and ν_{14}, assuming the vibrations are independent.

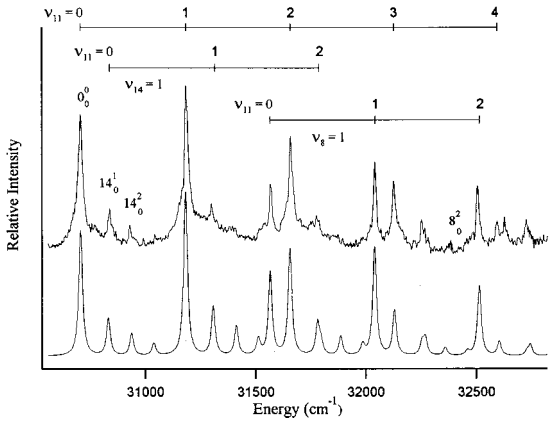

FIG. 5. Photodissociation spectrum of $[H_3C–Fe–OH]^+$ (upper trace). The spectrum shows progressions in the Fe–O stretch (ν_8), Fe–C stretch (ν_{11}), and O–Fe–C bend (ν_{14}). The bottom trace represents the simulated spectrum generated by convolution of Franck–Condon factors with a Lorentzian function with a width of 20 cm^{-1}.

IV. CONCLUSIONS

The spectroscopic characterization of $[H_2C{=}Fe–OH_2]^+$ and $[OH–Fe–CH_3]^+$, intermediates involved in the reaction of methane with bare FeO^+, have been reported for the first time. The vibronic features observed in the photodissociation spectrum of $[H_2C{=}Fe–OH_2]^+$ are identified as the result of photoexcitation of the $FeCH_2^+$ chromophore. From the spectroscopic threshold of $[H_2C{=}Fe–OH_2]^+ + h\nu \rightarrow FeCH_2^+ + H_2O$, an *upper limit* $D_o^0([H_2CFe–OH_2]^+) \leqslant 164\pm2$ kJ mol^{-1} is derived. The Fe–C bond length changes by 0.16 ± 0.02 Å upon photoexcitation. Comparison between the spectrum of $[H_2C{=}Fe–OH_2]^+$ and the two-photon spectrum of $FeCH_2^+$ reveals that $FeCH_2^+$ is less well solvated by water in the excited state than in the ground state. TD-DFT calculations predict that the vibrationally resolved progression in the spectrum of $[H_2C{=}Fe–OH_2]^+$ corresponds to a transition from the $2b_1$ $Fe^+–CH_2$ π-bonding orbital to the slightly antibonding Fe–C $7a_1$ orbital in the $FeCH_2^+$ chromophore. Thus, addition of a water molecule as a spectator in $[H_2C{=}Fe–OH_2]^+$ is shown to be a useful tool for the study of excited states of $FeCH_2^+$ lying below its dissociation threshold. The excellent agreement between the TD-DFT and the experimental results indicates that the TD-DFT methodology is a reliable tool in predicting excited electronic states of small transition-metal-containing systems.

The photodissociation spectrum of the insertion intermediate $[HO–Fe–CH_3]^+$ presents a vibrationally resolved band involving progressions in the excited state Fe–C stretch, Fe–O stretch, and O–Fe–C bend. Vibrational frequencies of 481 ± 1.0 cm^{-1} (and anharmonicity of 2.6 ± 0.2 cm^{-1}), 861 ± 3 cm^{-1}, and 132 ± 3 cm^{-1} were determined for the Fe–C stretch, Fe–O stretch and bend in the excited state, respectively. A Fe–C bond length change of 0.13 Å was calculated upon photoexcitation. Although time-of-flight mass spectrometry is not an ideal technique for the study of

isomeric species, the presence of distinguishable dissociation channels allow us to individually characterize the reaction intermediates $[H_2C{=}Fe{-}OH_2]^+$ and $[HO{-}Fe{-}CH_3]^+$.

ACKNOWLEDGMENT

Support for this work by a National Science Foundation Faculty Career Development Award is gratefully acknowledged.

[1] J. Haggin, Chem. Eng. News **71**, 27 (1993).
[2] R. H. Crabtree, Chem. Rev. **95**, 987 (1995).
[3] Y. Wang and K. Otsuka, J. Chem. Soc. Chem. Commun. **1994**, 2209 (1994).
[4] Y. Wang, K. Otsuka, and K. Ebitani, Catal. Lett. **35**, 259 (1995).
[5] R. Baum, Chem. Eng. News **72**, 24 (1994).
[6] K. Yoshizawa, J. Biol. Inorg. Chem. **3**, 318 (1998).
[7] A. C. Rosenzweig, C. A. Frederick, S. J. Lippard, and P. Nordlund, Nature (London) **366**, 537 (1993).
[8] W. B. Tolman, J. G. Bentsen, and S. J. Lippard, J. Am. Chem. Soc. **113**, 152 (1991).
[9] L. J. Shu, J. C. Nesheim, K. Kauffmann, E. Munck, J. D. Lipscomb, and L. Que, Science **275**, 515 (1997).
[10] S. Herold and S. J. Lippard, J. Am. Chem. Soc. **119**, 145 (1997).
[11] D. Lee and S. J. Lippard, J. Am. Chem. Soc. **123**, 4611 (2001).
[12] R. L. Rawls, Chem. Eng. News **79**, 23 (2001).
[13] D. Schröder and H. Schwarz, Angew. Chem. Int. Ed. Engl. **29**, 1433 (1990).
[14] D. Schröder and H. Schwarz, Angew. Chem. Int. Ed. Engl. **34**, 1973 (1995).
[15] D. Schröder, H. Schwarz, D. E. Clemmer, Y. Chen, P. B. Armentrout, V. Baranov, and D. K. Bohme, Int. J. Mass Spectrom. Ion Processes **161**, 175 (1997).
[16] K. Yoshizawa, Y. Shiota, Y. Kagawa, and T. Yamabe, J. Phys. Chem. A **104**, 2552 (2000).
[17] K. Yoshizawa, Y. Shiota, and T. Yamabe, J. Chem. Phys. **111**, 538 (1999).
[18] K. Yoshizawa, Y. Shiota, and T. Yamabe, Chem.-Eur. J. **3**, 1160 (1997).
[19] K. Yoshizawa, Y. Shiota, and T. Yamabe, J. Am. Chem. Soc. **120**, 564 (1998).
[20] D. Schröder, A. Fiedler, J. Hrusák, and H. Schwarz, J. Am. Chem. Soc. **114**, 1215 (1992).
[21] E. P. Hunter and S. G. Lias, in *NIST Chemistry WebBook, NIST Standard Reference Database Number 69*, edited by W. G. Mallard and P. J. Linstrom (National Institute of Standards and Technology, Gaithersburg, MD, 2000).
[22] P. B. Armentrout and B. L. Kickel, in *Organometallic Ion Chemistry*, edited by B. S. Freiser (Kluwer Academic, Dordrecht, The Netherlands, 1994).
[23] Y.-M. Chen, D. E. Clemmer, and P. B. Armentrout, J. Am. Chem. Soc. **116**, 7815 (1994).
[24] M. N. Glukhovtsev, R. D. Bach, and C. J. Nagel, J. Phys. Chem. A **101**, 316 (1997).
[25] G. L. Gutsev, B. K. Rao, and P. Jena, J. Phys. Chem. A **104**, 5374 (2000).
[26] C. J. Thompson, F. Aguirre, J. Husband, and R. B. Metz, J. Phys. Chem. A **104**, 9901 (2000).
[27] K. B. Wiberg, R. E. Stratmann, and M. J. Frisch, Chem. Phys. Lett. **297**, 60 (1998).
[28] N. N. Matsuzawa, A. Ishitani, D. A. Dixon, and T. Uda, J. Phys. Chem. A **105**, 4953 (2001).
[29] I. R. Farrell, J. van Slageren, S. Zalis, and A. Vlcek, Inorg. Chim. Acta **315**, 44 (2001).
[30] S. J. V. Gisbergen, J. A. Groeneveld, A. Rosa, J. G. Snijders, and E. J. Baerends, J. Phys. Chem. A **103**, 6835 (1999).
[31] T. Borowski and E. Broclawik, Chem. Phys. Lett. **339**, 433 (2001).
[32] J. Husband, F. Aguirre, P. Ferguson, and R. B. Metz, J. Chem. Phys. **111**, 1433 (1999).
[33] L. A. Posey, M. J. DeLuca, and M. A. Johnson, Chem. Phys. Lett. **131**, 170 (1986).
[34] M. Carleer, A. Jenouvrier, A.-C. Vandaele, P. F. Bernath, M. F. Mérienne, R. Colin, N. F. Zobov, O. L. Polyansky, J. Tennyson, and V. A. Savin, J. Chem. Phys. **111**, 2444 (1999).
[35] M. J. Frisch, G. W. Trucks, H. B. Schlegel *et al.*, GAUSSIAN 98, Revision A.3 (Gaussian, Inc., Pittsburgh, PA, 1998).
[36] J. Husband, F. Aguirre, C. J. Thompson, C. M. Laperle, and R. B. Metz, J. Phys. Chem. A **104**, 2020 (2000).
[37] J. M. Hollas, *High Resolution Spectroscopy* (Wiley, West Sussex, England, 1998).
[38] M. C. Holthausen, M. Mohr, and W. Koch, Chem. Phys. Lett. **240**, 245 (1995).
[39] R. L. Hettich and B. S. Freiser, J. Am. Chem. Soc. **108**, 2537 (1986).
[40] D. G. Musaev and K. Morokuma, Chem. Phys. **101**, 10697 (1994).
[41] F. Ogliaro, S. D. Loades, D. L. Cooper, and P. B. Karadakov, J. Phys. Chem. A **104**, 7091 (2000).
[42] F. Aguirre, Ph.D. thesis, University of Massachusetts, 2002.
[43] M. Okumura, L. I. Yeh, J. D. Meyers, and Y. T. Lee, J. Chem. Phys. **85**, 2328 (1986).
[44] T. Pino, N. Boudin, and P. Bréchignac, J. Chem. Phys. **111**, 7337 (1999).
[45] J. Qian, A. J. Midey, S. G. Donnelly, J. I. Lee, and J. M. Farrar, Chem. Phys. Lett. **244**, 414 (1995).
[46] J. Allison and D. P. Ridge, J. Am. Chem. Soc. **101**, 4998 (1979).
[47] See EPAPS Document No. E-JCPSA6-116-005210 for optimized geometries and calculated vibrational frequencies of the insertion intermediate, the aquo iron carbene intermediate and transition state TS2, as well as the relaxed potential energy surface scan along the O-Fe-C angle of the insertion intermediate. This document may be retrieved via the EPAPS homepage (http://www.aip.org/pubservs/epaps/html) or from ftp.aip.org in the directory /epaps/. See the EPAPS homepage for more information.